Journal of Cerebral Blood Flow & Metabolism (2014) 34, 1212–1222

www.jcbfm.com

ORIGINAL ARTICLE

Role of microRNA29b in blood–brain barrier dysfunction during hyperhomocysteinemia: an epigenetic mechanism

Anuradha Kalani, Pradip K Kamat, Anastasia Familtseva, Pankaj Chaturvedi, Nino Muradashvili, Nithya Narayanan, Suresh C Tyagi and Neetu Tyagi

Although blood–brain barrier (BBB) integrity is maintained by the cross-talk of endothelial cells, junction proteins, and neurogliovascular network, the epigenetic mechanisms behind BBB permeability are largely unknown. We are reporting for the first time miR29b-mediated regulation of BBB, which is a novel mechanism underlying BBB integrity. We hypothesize that miR29b regulates BBB dysfunction by regulating DNMT3b, which consequently regulates the levels of metalloproteinases, that can eat up the membrane and junction proteins leading to leaky vasculature. In addition, 5′-azacytidine (5′-aza) was used to test its efficacy on BBB permeability. Blood–brain barrier disruption model was created by using homocysteine, and in the models miR29b was identified to be most affected, by using microRNA RT^2-qPCR array. MiR29b mimics and inhibitors also confirmed that miR29b regulates the levels DNMT3b and MMP9. In hyperhomocysteinemic cystathionine-β-synthase deficient (CBS$^{+/-}$) mice with high brain vessel permeability, miR29b levels were also high as compared with wild-type (WT) mice. Interestingly, 5′-aza improved BBB permeability by decreasing the expression of miR29b. In conclusion, our data suggested miR29b-mediated regulation of BBB dysfunction through DNMT3b and MMP9. It also potentiates the use of microRNAs as candidates for future epigenetic therapies in the improvement of BBB integrity.

Journal of Cerebral Blood Flow & Metabolism (2014) **34,** 1212–1222; doi:10.1038/jcbfm.2014.74; published online 7 May 2014

Keywords: 5′-azacytidine; blood–brain barrier; endothelial cells; homocysteine; microRNA

INTRODUCTION

Cerebral microvessels form the major interface between the blood and brain, termed as blood–brain barrier (BBB), which separates brain from the circulatory system. It is formed by tightly packed endothelial cells that line the cerebral brain vessels. Their structure is maintained through specialized tight junctions, gap junctions, and adherent junctions.[1,2] The barrier is important for various aspects such as: selective transportation of the molecules into and out of the brain, preventing entry of harmful substances to the brain, allowing specific ion transporter channels to regulate ionic traffic, and maintenance of the brain integrity.[2] The BBB disruption can lead to increased permeability, which is an important factor in vascular etiology and stroke-like pathology.[2,3]

Although, the BBB is exclusively maintained by junction proteins like zonula occludens, claudins, and cadherins,[4] studies demonstrating the role of microRNAs in regulating BBB remain scarce. We are for the first time, reporting the role of miR29b in regulating BBB permeability and dysfunction. The miR29 family is the 'epi-miR' that regulates epigenetic processes and there are four members reported of this family: miR29a and miR29b1 (which is processed through chromosome no. 7), and miR29b2, miR29c (that is co-transcribed from chromosome no. 1). Mounting reports suggest specific role of miR29b in DNA methylation by directly targeting DNMT genes[5,6] although, these reports are in lung cancer and leukemia. There have been contrasting reports regarding the role of miR29b in ischemic brain injury. One of the earlier reports suggests that downregulation of miR29b after acute ischemic stroke contributes to neural cell death and infarct size.[7] However, one report describes that upregulation of miR29b after ischemic brain injury promotes neuronal cell death by inhibiting Bcl2L2.[8] As these studies do not throw light on the role of miR29b in BBB disruption and reports about this microRNA are lacking, the significance of our study lies in drawing a clear picture on how miR29b can affect BBB.

Homocysteine (Hcy) is a sulfur-containing amino acid, derived from methionine metabolism, and its elevated level in plasma is referred to as hyperhomocysteinemia (HHcy). We have used Hcy to create BBB disruption model in bEnd.3 cells for *in vitro* studies and cystathionine-β-synthase deficient (CBS$^{+/-}$) gene-deficient mouse model for *in vivo* studies. It has been reported that subclinical elevation in Hcy levels (from baseline of $\sim 3\,\mu$mol/L to $\sim 12\,\mu$mol/L) results in considerable leakage of plasma proteins (albumin and endogenous immunoglobulins) in rodent brains.[9–11] We earlier reported that CBS$^{+/-}$ mice have high levels of Hcy ($21 \pm 4\,\mu$mol/L) as compared with WT ($5 \pm 2\,\mu$mol/L).[12] Homocysteine instigates BBB disruption by inducing redox stress and upregulating matrix metalloproteinases (MMPs), which are zinc-dependent endopeptidases that have a critical role in matrix remodeling and lead to blood–endothelial barrier leakage.[13] In addition, the contribution of high Hcy levels to BBB dysfunction lies in modulating DNA methylation by donating methyl groups through *s*-adenosylmethionine (which is a universal methyl donor) and mediating methylation of important genes and histones.[14] Creating BBB disruption by Hcy, we questioned whether miR29b can ameliorate this condition by mitigating the MMPs expression and DNA methylation.

Department of Physiology and Biophysics, School of Medicine, University of Louisville, Louisville, Kentucky, USA. Correspondence: Dr N Tyagi, Department of Physiology and Biophysics, 500 South Preston Street, Health Sciences Centre, A-1201, University of Louisville, Louisville, KY 40202, USA.
E-mail: n0tyag01@louisville.edu
The work was supported by National Institutes of Health grants HL107640 to NT.
Received 4 December 2013; revised 4 March 2014; accepted 25 March 2014; published online 7 May 2014

5′-Azacytidine (5′-aza; an epigenetic agent) has been used in alleviating neurologic outcomes and stroke infarct volume.[15,16] As some preliminary reports state that miR29b levels can be affected by the treatment with 5′-azacytidine or decitabine,[17,18] it was very interesting to see whether 5′-aza can improve BBB permeability and what role miR29b has in 5′-aza-mediated permeability mitigation. Hence, we hypothesize that miR29b regulates BBB permeability by regulating these sequential events; (1) it regulates the levels of DNMT3b, (2) DNMT3b in turn regulates MMP9 levels, which are proteases and can cleave BBB junctions and form leaky vasculature, (3) MMP9 alter the junction proteins (occludens, claudins, and cadherins) and, (4) owing to alteration in junction proteins, the BBB permeability is affected. To validate the hypothesis, we used Hcy and 5′-aza in parallel and examined the events like permeability, reactive oxygen species generation, expression of MMP9, DNMTs, and junction proteins along with the expression of miR29b by using miR29b mimics and inhibitors.

MATERIALS AND METHODS

Cell Culture

Mouse brain endothelial cell line (bEnd.3) was purchased from American Type Culture Collection (ATCC, Manassas, VA, USA) and grown in Dulbecco's modified Eagle's medium supplemented with 4.5 g/L glucose, 3.7 g/L sodium bicarbonate, 4 mmol/L glutamine, 10% fetal bovine serum, 100 U/mL penicillin, and 100 μg/mL streptomycin, pH 7.4. The cells were maintained under an atmosphere of 5% CO_2 and 95% air in 25 cm^2 tissue culture flask. The cells were allowed to grow to 70% to 80% confluence, trypsinized, and seeded onto six-well plate and given treatments.

Treatment Groups

In vitro. The bEnd.3 cells were used for *in vitro* study as described by previous studies[19,20] and given the following treatments: (1) Control (no treatment), (2) Hcy (100 μmol/L), (3) Hcy + 5′-aza (10 μmol/L), 4) 5′-aza. Cells were given treatment for 24 hours and harvested for further experiments.

In vivo. Experimental male mice (age 8 to 10 weeks) groups of the study were as following: (1) C57BL/6 (wild type, WT), (2) C57BL/6 treated with 5′-aza (WT + 5′-aza), (3) $CBS^{+/-}$, genetic HHcy mice, (4) $CBS^{+/-}$ mice treated with 5′-aza ($CBS^{+/-}$ + 5′-aza). The 5′-aza (0.5 mg/kg body weight) treatments were given through intraperitoneal route for a period of 6 weeks at alternate days. The animal procedures were carefully reviewed and approved by the Institutional Animal Care and Use Committee, University of Louisville, in accordance with the animal care and proper guidelines of the National Institutes of Health.

Creating Blood–Brain Barrier Cell Permeability Models in Cell Line and Mouse

Endothelial cell permeability was created by treating the cells with 100 μmol/L Hcy. We did a dose-dependent permeability assay using transwell migration supports in bEnd.3 cells and found that 100 μmol/L Hcy to be threshold concentration for developing endothelial cell permeability. We also did a dose-dependent treatment for 5′-aza and found that 10 μmol/L 5′-aza decreased permeability significantly. Permeability was assessed using Lucifer yellow, BSA-647, and fluorescein isothiocyanate labelled bovine serum albumin (FITC-BSA) as described earlier.[21,22] Briefly, the cells were grown on transwell permeable supports (Corning, Corning, NJ, USA) with polycarbonate membranes (Nuclepore Track-Etched membrane; 6.5 mm in diameter, 0.4-μm pore size, and pore density of 108/cm^2). After treatment with Hcy and 5′-aza, the media was collected from bottom chamber at different time intervals (Lucifer yellow and BSA-647) and overnight (FITC-BSA). Extent of leaked BSA through a membrane was assessed by measuring fluorescence intensity in the samples with microplate reader (SpectraMax M2; Molecular Devices, Sunnyvale, CA, USA).

The use of $CBS^{+/-}$ mice in this study as model for BBB disruption was in agreement with our previous study.[23] Briefly, mouse was anesthetized and placed on a stereotaxic apparatus (World Precision Instruments, Sarasota, FL, USA). Craniotomy was done over the parietal cranial bone above the left hemisphere and around 14-mm window was made in the skull using high-speed microdrill (Fine Science Tools, Foster City, CA, USA). Carotid artery cannulation was done for infusion of 300 mg/mLFITC-BSA. Fluorescein isothiocyanate labelled bovine serum albumin (BSA, 0.2 mL/100 g of body weight) was infused through the carotid artery cannulation by a syringe pump (Harvard Apparatus, Holliston, MA, USA) and allowed to circulate. The images were captured and the data were interpreted with software provided with the instrument and Image-pro plus 6.3 (Media Cybernetics, Rockville, MD, USA).

Measurement of Reactive Oxygen Species Thorough Confocal and Flow Cytometry

The intracellular reactive oxygen species generation was measured by treating the cells with 2′-7′-dichlorodihydrofluorescein diacetate (H_2DCF-DA, 5 μmol/L, Invitrogen, Carlsbad, CA, USA) as described earlier.[24] Briefly, cells were incubated with the dye for 20 minutes at 37°C, washed with phosphate-buffered saline, and analyzed through laser scanning confocal microscope (× 60, and × 100 objective, FluoView 1000; Olympus, Center Valley, PA, USA). For flow cytometry, the cells were scrapped and subjected to Accuri's C6 Flow Cytometer (Accuri Cytometers, Ann Harbor, MI, USA).

Quantitative Real-Time PCR for MicroRNA and Individual Genes

RNA was isolated using miRNeasy Mini Kit (Qiagen, Valencia, CA, USA) as per manufacturer's instructions and converted to cDNA using miScript II RT kit (Qiagen). The RT^2-qPCR array was performed on 96-well plates (MIMM-107ZA-2, miScript miRNA PCR array, mouse neurologic development and disease, Qiagen) as per manufacturer's instructions. The cDNA was also analyzed for individual microRNA expression using miScript SYBR Green PCR kit. The amplification was performed in Stratagene Mx3000p (Agilent Technologies, Santa Clara, CA, USA) and the CT values were determined after baseline and threshold adjustment and the results are expressed in fold expression. The transcript levels of DNMT3b, MMP9 were also determined and the gene expression was normalized with Rn18s. Supplementary Table 1 describes primer sequences used in the study.

Sodium Dodecyl Sulfate Polyacrylamide Gel Electrophoresis and Western Blotting

Protein extracts (40 μg) were separated in polyacrylamide gel and transferred to polyvinylidene difluoride membranes using electrotransfer apparatus (Bio-Rad, Hercules, CA, USA). The membranes were blocked with 5% non-fat dry milk (1 hour) and probed with primary antibody (1:1,000) overnight at 4°C. Next day, membrane was washed and incubated with secondary antibody (-HRP conjugated, 1:10,000) for 60 minutes at room temperature, and developed with ECL detection system (GE Healthcare, Piscataway, NJ, USA). The images were recorded in chemi-program of the gel documentation system (Bio-Rad) and band intensity was normalized with respective glyceraldehyde 3-phosphate dehydrogenase intensity calculated through Image Lab densitometry software (Bio-Rad).

Gelatin Zymography Assay

A quantity of 30 μg protein sample was run on 10% sodium dodecyl sulfate polyacrylamide gel electrophoresis gel prepared with 2% gelatin,[25] washed thrice with 2.5% Triton X-100 (20 minutes each), and incubated for 24 hours (37°C) in activation buffer (5 mmol/L Tris–HCl (pH 7.4), 0.005% (v/v) Brij-35, and 1 mmol/L $CaCl_2$). Gels were Coomassie stained and distained to monitor proteolytic activity of the sample as a clear band on a stained background. The images were recorded with gel documentation system (Bio-Rad) and the data were analyzed with the Image Lab software (Bio-Rad).

Transfection of bEnd.3 Cells and *In Vivo* Administration of Anti-miR29b

The bEnd.3 cells were transfected with miScript miR29b Mimics (MSY0000127 cat# 219600-S0), miScript miR29b inhibitor (MIN0000127 cat# 219300-S0P4), DNMT siRNA (cat# SI00165382) along with all-star negative control siRNA, and miScript negative control inhibitor (cat# 1027280 and cat# 1027271, Qiagen), using HiPerFect transfection reagent (cat# 301702, Qiagen) as recommended by the supplier's protocol.

Locked nucleic acid-mediated silencing of microRNA was performed according to previous reports.[26,27] CBS$^{+/-}$ mice were administered with locked nucleic acid scramble miR and locked nucleic acid-anti-miR29b intracerebrally suspended in artificial cerebrospinal fluid (800 ng/2 μL). The method of intracerebral administration was followed by our previous report.[28] The mice were used for FITC-BSA leakage analysis after 24 hours of anti-miR29 administration.

Immunohistochemistry Analysis

A quantity of 20 μm frozen brain tissue section was cut (Cryostat, Leica, CM, USA) and mounted on charged slides (VWR, West Chester, PA, USA). The sections were blocked with blocking solution (0.1% Triton X-100 TBS (TBS-T), 0.5% BSA, and 10% normal donkey serum; 1 hour) and incubated with primary antibody (1:100) for overnight at 4°C. Sections were washed

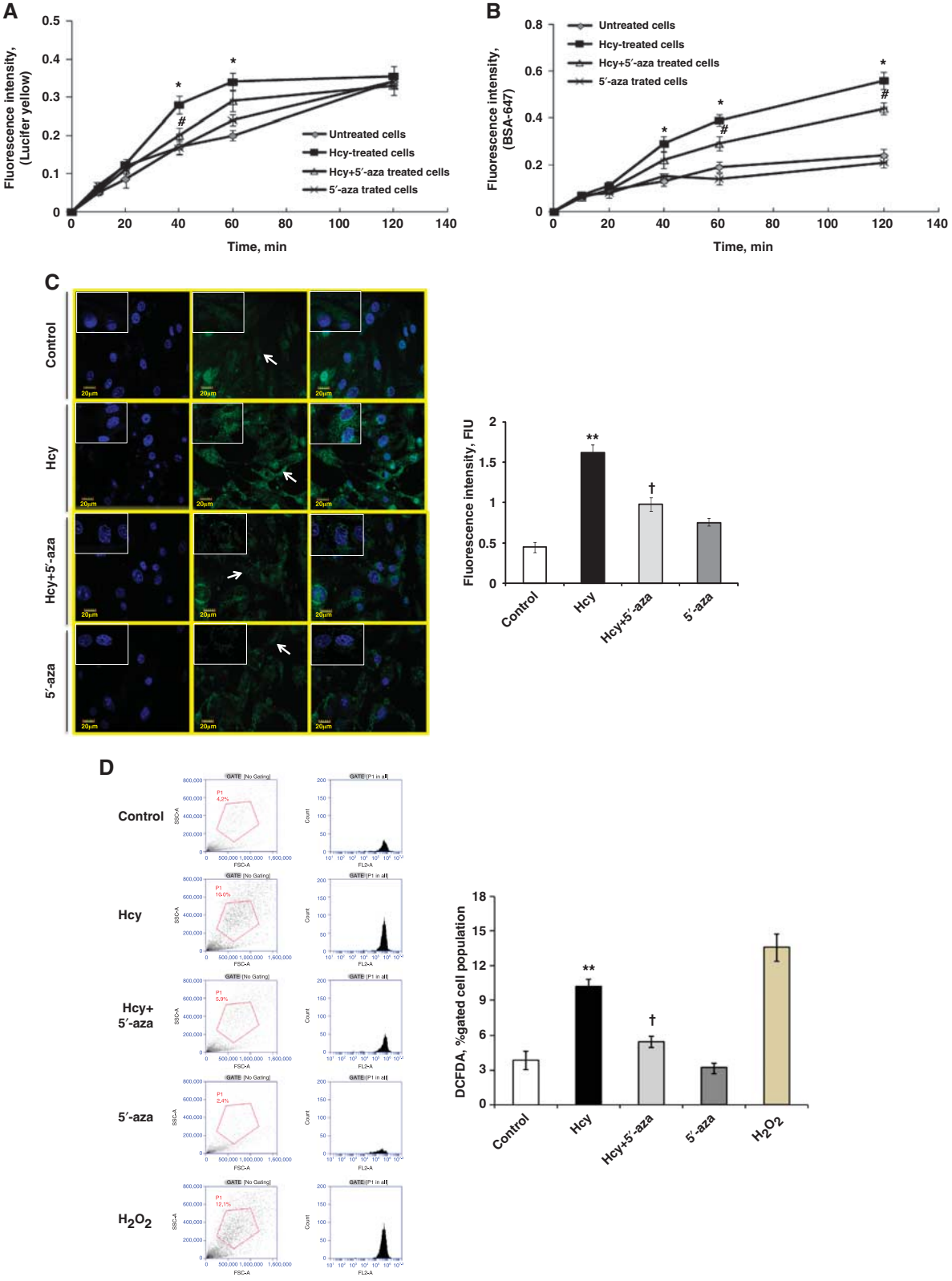

thrice with TBS, incubated with corresponding fluorescent dye-conjugated secondary antibodies (60 minutes), stained with 4′,6-diamidino-2-phenylindole (1:10,000), and mounted with anti-fade mounting media. Images were acquired using a laser scanning confocal microscope ($\times 60$ objectives, FluoView 1000; Olympus). Total fluorescence intensity in five random fields (for each experiment) was measured with image analysis software (Image-Pro Plus; Media Cybernetics).

Statistical Analysis

All values are expressed as mean ± s.e.m. Interaction between groups was determined by two-way analysis of variance test (for three or more groups). Two tailed Student's *t*-test was used for 2-group comparisons using SPSS software (ver.17). The null hypothesis was rejected at '*P*'-value equal to or less than 0.05.

RESULTS

Confirming Blood–Brain Barrier Disruption in bEnd.3 Cells and Hyperhomocysteinemic Mouse Models

Homocysteine-induced BBB disruption model in bEnd.3 cells was confirmed by analyzing paracellular and transcellular transport systems using Lucifer yellow and BSA-647 fluorescence probes leakage at different time points (10, 20, 40, 60, 120 minutes) in four treatment groups. In Hcy-treated cells, significant endothelial cell permeability was observed, as evident through increased leakage of the Lucifer yellow (at 40 minutes and 60 minutes; Figure 1A) and BSA-647 (at 40 minutes to 120 minutes; Figure 1B) fluorescent dyes, which suggested that both paracellular and transcellular transport systems are affected during endothelial disruption. 5′-azacytidine significantly decreased Hcy-induced endothelial disruption at different time points. 5′-azacytidine alone did not affect endothelial cell integrity (for Figure 1A, $F > F_{\_crit}$, $F = 94.52$, $P < 0.0001$; for Figure 1B, $F > F_{\_crit}$, $F = 109.35$, $P < 0.0001$).

As oxidative stress is a hallmark of permeability, we estimated oxidative stress in cells using H_2DCF-DA dye. We found increase in oxidative stress in Hcy-treated cells as compared to control using confocal microscopy (Figure 1C). However, the oxidative stress in the Hcy-treated cells was decreased with 5′-aza treatment. The results were also confirmed by using flow cytometry for H_2DCF-DA-treated cells and we found similar results (Figure 1D). H_2O_2 was used as positive control for flow cytometry analysis (Figure 1D).

In CBS$^{+/-}$/HHcy mouse models, BBB disruption was confirmed by macromolecular permeability analysis. Out of the four groups, HHcy mice revealed high pial venular leakage as compared to WT (Figure 2). In WT + 5′-aza and CBS$^{+/-}$ + 5′-aza groups, the permeability was not affected and was comparable with the WT group (Figure 2).

Identification and Assessment of miR29b in Blood–Brain Permeability Model

The RT^2-qPCR array was used to explore microRNAs induced under BBB disruption, and we determined several fold increase in different microRNAs along with significant increase in miR29 family members (miR29a-3, miR29b-3, and miR29c-3) as compared to control cells (Figure 3A). The individual miR assay, with snoRD72 as endogenous control, also determined significant increase in miR29 family members (miR29a, miR29b1, miR29b2, and miR29c) in Hcy-treated cells. Interestingly, 5′-aza significantly downregulated Hcy-induced miR29b1 and miR29b2 (Figure 3B).

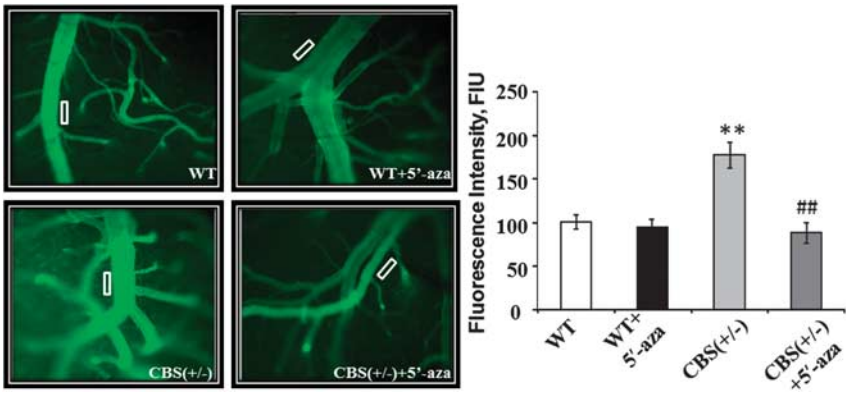

Figure 2. Blood–brain barrier (BBB) disruption in hyperhomocysteinemic mice models. Representative recorded images showing macrovascular leakage through brain pial venules using fluorescein isothiocyanate labelled bovine serum albumin. Intensity data was calculated at the rectangular block, as area of interest shown on the images (white block), and expressed as fluorescence intensity units (FIU) in the bar diagram. Cystathionine-beta-synthase-deficient (CBS$^{+/-}$) mice showed high permeability as compared with wild type (WT), WT + 5′-aza (5′-azacytidine), and CBS$^{+/-}$ + 5′-aza groups. Data represent mean ± s.e.m. $^{**}P < 0.005$ versus WT; $^{\#\#}P < 0.005$ versus CBS$^{+/-}$ mice groups ($n = 3$).

Figure 1. Blood–brain barrier (BBB) disruption and hyperhomocysteinemia-induced oxidative stress in bEnd.3 cells. (**A**, **B**) Blood–brain barrier model confirmation in bEnd.3 cells using Lucifer yellow (**A**) and Alexa Fluor 647-conjugated bovine serum albumin (BSA) (BSA-647) (**B**) fluorescent dyes. Cells were treated with homocysteine (Hcy) (100 μmol/L) to attain permeability model, while 5′-azacytidine was used to rescue the endothelial cell leakage. Lucifer yellow reports paracellular transport while BSA-647 represents paracellular and transcellular transports. (**C**) Confocal analysis showing oxidative stress in bEnd.3 cells using 2′-7′-dichlorodihydrofluorescein diacetate (H_2DCF-DA) fluorescent dye. Green color intensity is the representation of oxidative stress as indicated by arrows. Blue color represents cell nuclei stained with 4′,6-diamidino-2-phenylindole. All images were taken at $\times 60$ magnification while inset images were taken at $\times 100$ magnification. Bar diagram represents H_2DCF-DA fluorescent intensity in different cell treatment groups. (**D**) Flow cytometry showing oxidative stress using H_2DCF-DA fluorescent intensity in bEnd.3 cells. The first lane shows the forward scattered plot with gating applied, and the second lane shows the count number in terms of peak area. The live cell count ($\sim 2 \times 10^6$) was first determined by Bio-Rad TC10 automated cell counter using trypan blue dye. The extent of oxidative stress is also represented in bar graph expressed in terms of H_2DCF-DA, percentage-gated cell population. Data represent mean ± s.e.m. $^{*}P < 0.05$, $^{**}P < 0.005$ versus control; $^{\#}P < 0.05$, $^{\dagger}P < 0.05$ versus Hcy-treated cells; data analyzed from four independent experiments ($n = 4$).

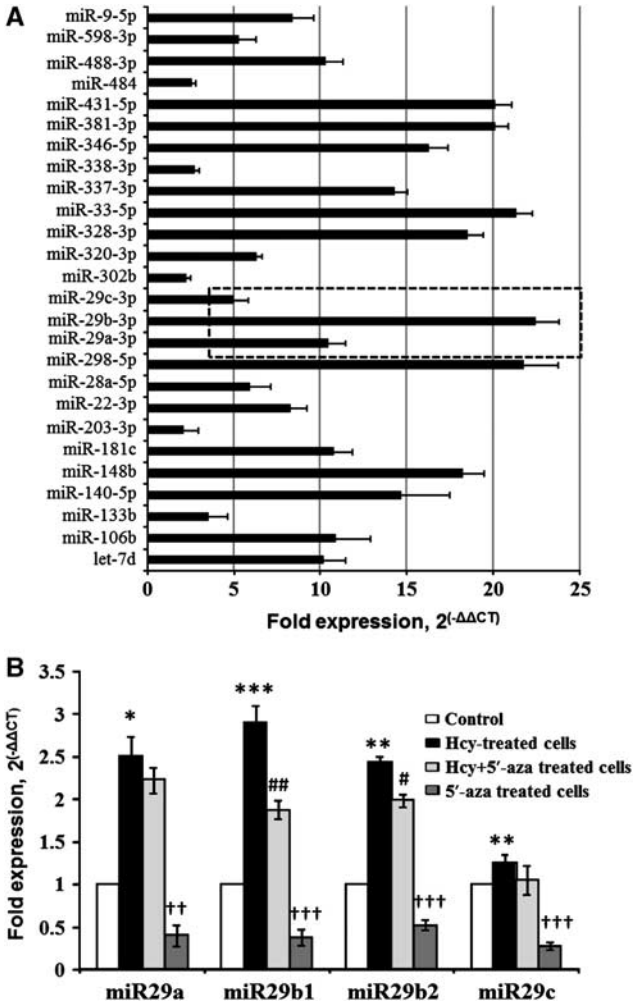

Figure 3. Identification of miR29b in blood–brain barrier disruption by using RT^2-qPCR microRNA array. (**A**) RT^2-qPCR array determined altered expression of different microRNAs in BBB disruption model in bEnd.3 cells (treated with 100 μmol/L of homocysteine (Hcy)) as compared with control, and the results are represented through horizontal bar graph. Dotted inset is showing upregulation of miR29 family. (**B**) Bar graph representing qPCR analyses of individual miR29 family members (miR29a, miR29b1, miR29b2, and miR29c) in bEnd.3 cells treated with Hcy (100 μmol/L), and 5′-azacytidine (10 μmol/L). Data represent mean ± s.e.m. $^*P<0.05$, $^{**}P<0.005$, $^{***}P<0.0005$ versus control; $^{\#}P<0.05$, $^{\#\#}P<0.05$, $^{\dagger\dagger}P<0.005$, $^{\dagger\dagger\dagger}P<0.0005$ versus Hcy-treated cells; data analyzed from four independent experiments ($n=4$).

Regulation of miR29, DNMT3b, and MMP9 in bEnd.3 Cells during Blood–Brain Barrier Permeability

To confirm Hcy-induced expression of miR29b, we tested different doses of Hcy and found a dose-dependent increase in miR29b expression (Figure 4A). We further looked into the downstream events and checked the expression of DNMT3b and MMP9 with increasing doses of Hcy. We found decrease in the DNMT3b protein expression with increase in Hcy, but not in DNMT3a (Figure 4B). Conversely, we found increase in the protein expression and activity of MMP9 on western blot and gelatin Zymography (Figure 4C). Connecting these three dots, with increase in Hcy, we found increase in miR29b and MMP9 along with decrease in DNMT3b. In parallel to Hcy, we also tested dose-dependent effect of 5′-aza on MMP9 levels and found that high levels of 5′-aza reduced the expression and activity of MMP9 (Figure 4D).

Use of miR29b Mimics and Inhibitors to Confirm the Regulation of DNMT3b and MMP9

We transformed the cells with miR29b mimics and inhibitors and checked the expression of DNMT3b and MMP9 with real-time PCR. In cells transformed with miR29b mimics, the mRNA expression of DNMT3b significantly diminished as compared with scramble, upon Hcy treatment (Figure 5A) ($F>F_{\_crit}$, $F=169.3$, $P<0.0001$). While with the use of anti-miR29b, the mRNA levels of DNMT3b increased profoundly. Conversely, the expression of MMP9 increased fourfold with the use of mimics and decreased to 0.5-folds with the use of inhibitors with Hcy treatment (Figure 5B) ($F>F_{\_crit}$, $F=176.3$, $P<0.0001$). To further confirm the regulation of MMP9 with miR29, we checked the MMP9 protein expression with western blot and MMP9 activity with gelatin Zymography {Figure 5C ($F>F_{\_crit}$, $F=8.699$, $P<0.0003$), 5D ($F>F_{\_crit}$, $F=17.94$, $P<0.0001$)}. We found similar results as with real-time PCR. With miR29b mimics the expression and activity of MMP9 increased, while the results were reversed with miR29b inhibitors (Figures 5C and D). We used 5′-aza in parallel with Hcy in all the experiments and found that 5′-aza reverted back the effects of Hcy and ameliorated the levels of DNMT3b and MMP9 (Figure 5A–D).

The Effects of Mimics and Inhibitors on Cell Permeability

We checked the effects of miR29b mimics and inhibitors directly on the cell permeability by FITC-BSA transwell migration assay and found that miR29b mimics significantly increased the cell permeability in Hcy-treated cells as compared with control (Figure 5E). MiR29b inhibitor decreased the Hcy-induced permeability (Figure 5E). 5′-aza co-treated with Hcy decreased the permeability in the untransformed cells and miR29b transformed cells. 5′-Azacytidine alone did not alter the permeability in transformed and untransformed cells as compared with control (Figure 5E) ($F>F_{\_crit,}$ $F=8.467$, $P<0.0001$).

miR29b, DNMT3b, and MMP9 Regulation in Mice Brain Tissues

In mice model with HHcy CBS$^{+/-}$, we found increase in the expression of miR29b as compared with WT with real-time PCR (Figure 6A), which correlated with the *in vitro* data. The levels of miR29b were significantly decreased in CBS$^{+/-}$ mice treated with 5′-aza and became comparable with WT + 5′-aza. The protein expression of DNMT3b decreased in CBS$^{+/-}$ mice as compared with WT (Figure 6B). The expression and activity of MMP9 were increased in the CBS$^{+/-}$ groups as compared with the control group (Figures 6C and D). While the expression/activity of MMP9 was significantly decreased in CBS$^{+/-}$ mice treated with 5′-aza (Figures 6C and D).

Analysis of Molecular and Junction Protein Alterations Maintaining Blood–Brain Barrier Permeability

Brain tissue expressions of endothelial marker (CD31), gap junction (connexin40), tight junction (occludin), and adherent junction (VE-cadherin) were determined in BBB disruption with immunohistochemistry analysis. Confocal analysis showed significant reduced intensity of CD31, VE-cadherin, occludin, and increased intensity of Connexin40 in CBS$^{+/-}$ as compared with WT − and WT + 5′-aza brain vessels (Figure 7A–D). The treatment of 5′-aza to CBS$^{+/-}$ mice significantly ameliorated CD31 and VE-cadherin expressions, as compared with CBS$^{+/-}$ brain cortical vessels (Figures 7A, C, and D). In addition to this, we also determined oxidative stress (Nox-4), endothelial dysfunction (eNOS), and synaptic plasticity (SAP-97) markers in treated/untreated CBS$^{+/-}$ and WT − brains. Nox-4 was increased, while eNOS and SAP-97 were significantly decreased in HHcy brain as compared with WT and WT + 5′-aza brains (Figure 7E). However,

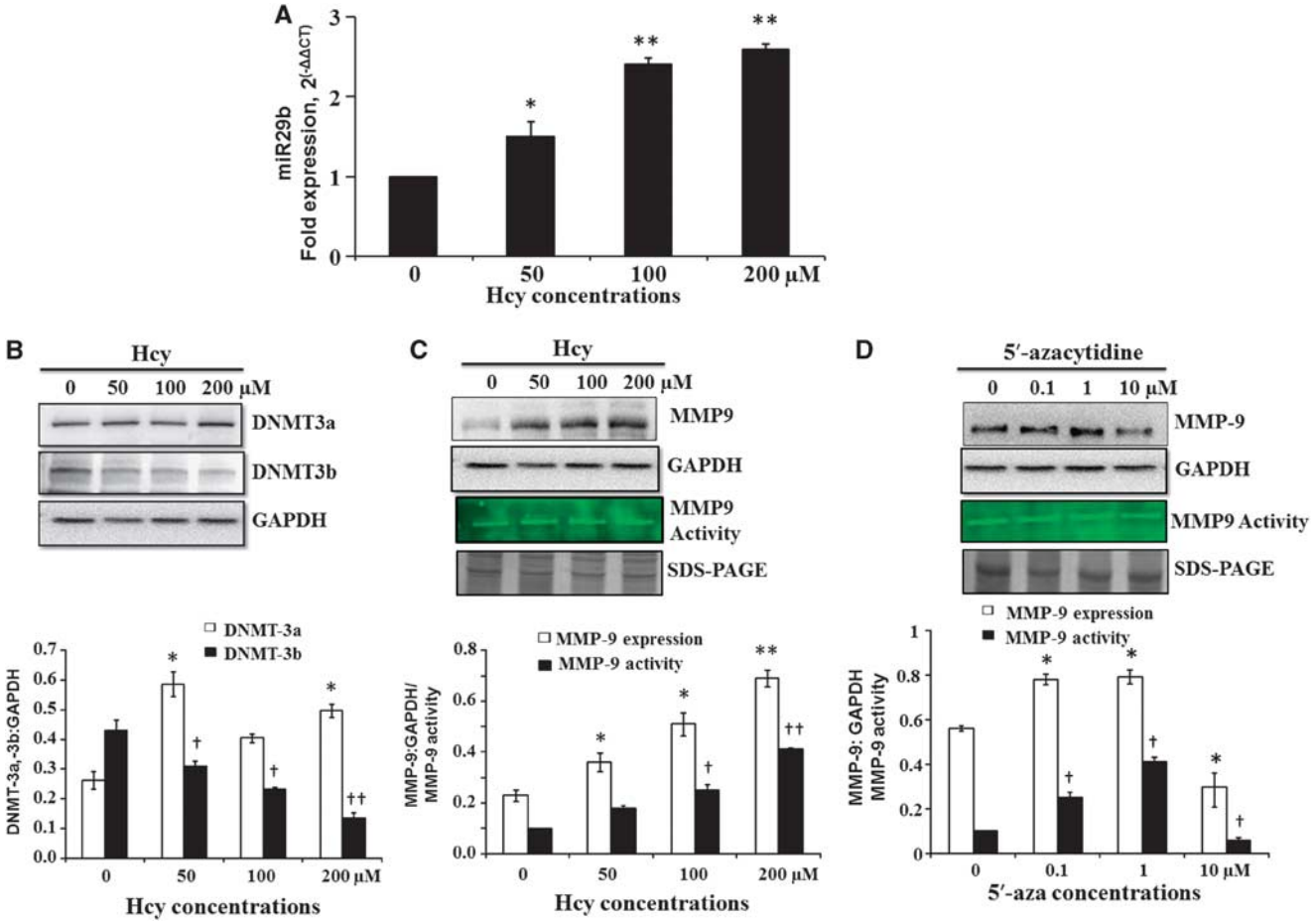

Figure 4. miR29b, DNMT3b, and MMP9 regulation during blood–brain permeability in bEnd.3 cells. (**A**) Bar graph showing dose-dependent increase in miR29b with increasing dose of homocysteine (Hcy) (0, 50, 100, 200 μmol/L) treatment. (**B**) Representative images of western blot showing expressions of DNMT3a and DNMT3b at different concentrations of Hcy. Protein expressions are normalized with their respective glyceraldehyde 3-phosphate dehydrogenase (GAPDH) controls and the results are also dictated by bar diagram. (**C**) Western blot image showing expressions of MMP9 and gelatin zymograph image of MMP9 activity at different concentrations of Hcy. The results are also expressed in bar graph showing MMP9 band intensity, normalized with GAPDH band intensity, and gelatin degradation activity of MMP9. (**D**) Western blot and gelatin zymograph images showing MMP9 levels at different concentrations of 5′-azacytidine (0, 0.1, 1, 10 μmol/L). Results are also dictated by bar graph showing MMP9 protein expression (normalized with respective GAPDH), and its activity. Data represent mean ± s.e.m. $^{*}P<0.05$, $^{**}P<0.005$; $^{\dagger}P<0.05$, $^{\dagger\dagger}P<0.005$ versus control; data analyzed from four independent experiments ($n=4$).

treatment with 5′-aza alleviated these markers in CBS$^{+/-}$ + 5′-aza brain (Figure 7E).

DISCUSSION

The studies on the role of epigenetic remodeling in brain vascular pathology are scarce and hence, this report dictates the involvement of microRNAs in cerebrovascular leakage. The results suggest that miR29b regulates BBB permeability by affecting endothelial cells and regulating the levels of MMP9 through DNMT3b. The use of miR29b mimics showed increase in the BBB permeability thereby affecting endothelial cells along with elevated expression of MMP9 and diminished DNMT3b, which was reversed by using miR29b inhibitors. This confirmed the BBB regulation with miR29b with the involvements of DNMT3b and MMP9. Interestingly, when we used 5′-aza, it mitigated the BBB disruption by alleviating the levels of MMP9, DNMT3b, and miR29b.

Clinical reports suggest that mild–to-moderate HHcy occurs in 5% to 10% of the general population, 40% of patients with peripheral vascular disease, and may reach greater than 90% in patients on hemodialysis.[29,30] Previous studies from our and other labs have also shown that high Hcy levels impart significant influence in BBB opening and thus raise permeability.[3,31–33] Therefore, we created BBB disruption model by using Hcy in bEnd.3 cells and to validate *in vitro* findings, we used genetically hyperhomocysteinemic CBS$^{+/-}$ mice models for *in vivo* studies. Previous studies also described bEnd.3 cells as a convenient and useful model to study BBB functions.[19,20] The BBB disruption was reflected by transwell migration assay in cell line and brain pial venules permeability in CBS$^{+/-}$ mice model. There was increase in the production of reactive oxygen species in the two BBB models, which is one of the factors for BBB disruption as reflected through previous reports.[23,24] In BBB permeability, we checked the levels of microRNAs and observed profound increase in the levels of miR29 family in miR RT^{2}-qPCR array. Literature suggests that miR29b can target DNMTs and indirectly affect methylation of genes. Fabbri *et al.*[5] have reported that miR29b binds to the 3′-UTRs of DNMT3a, and -3b (*de novo* methyl transferases), two key enzymes involved in DNA methylation, and reverts aberrant methylation in lung cancer. Similarly, Takada *et al.*[34] identified DNMT3a and DNMT3b as targets of miR29b and found that these two DNMTs are negatively regulated by miR29b in primordial germ cells of female mouse embryos. In our study in brain, we

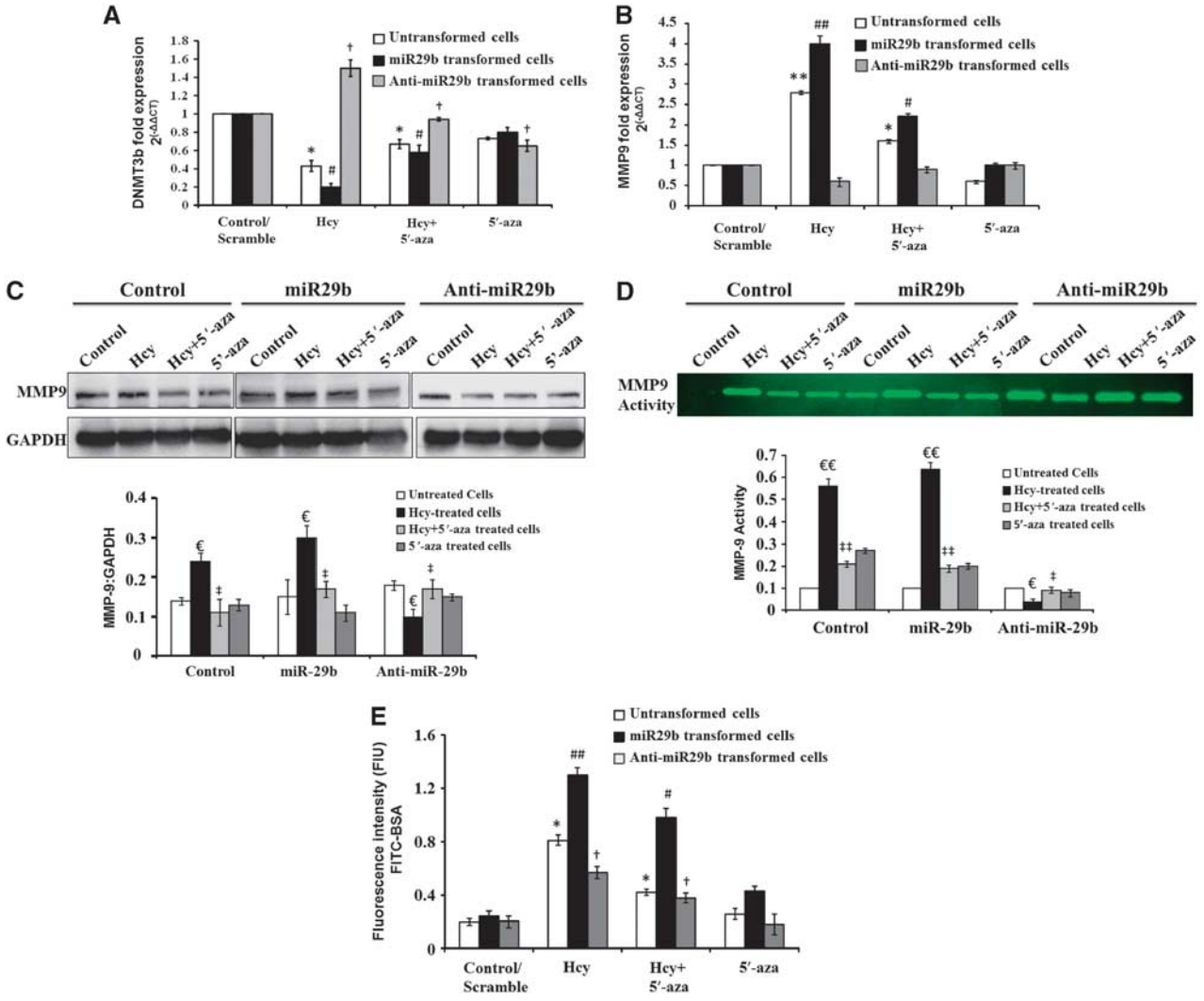

Figure 5. Use of miR29 mimics and inhibitors to confirm the regulation of DNMT3b and MMP9 in bEnd.3 cells. (**A**) Bar diagram depicting DNMT3b messenger RNA (mRNA) levels in transfected cells (miR29b and anti-miR29b) along with untransfected cells, treated with homocysteine (Hcy) and 5′-azacytidine (5′-aza). The results are normalized with Rn18s mRNA levels. (**B**) Similarly, qPCR analysis of MMP9 mRNA expression is depicted through bar graph and the results are normalized with Rn18s. (**C**, **D**) Western blot C and gelatin zymograph D results of MMP9 levels in transfected cells (miR29b and anti-miR29b) along with untransfected cells treated with Hcy and 5′-aza. (**E**) Bar graph showing endothelial cell permeability using fluorescein isothiocyanate labelled bovine serum albumin in transfected and untransfected cells treated with Hcy and 5′-aza. Data represent mean ± s.e.m. $^{*}P<0.05$, $^{**}P<0.005$ versus untransformed control; $^{\#}P<0.05$, $^{\#\#}P<0.005$ versus scramble for miR29b; $^{\dagger}P<0.05$ versus scramble for anti-miR29b; $^{€}P<0.05$, $^{€€}P<0.005$ versus control/scramble; $^{‡}P<0.05$, $^{‡‡}P<0.005$ versus Hcy-treated cells; data analyzed from three independent experiments ($n=3$).

found dose-dependent increase in the expression of miR29b with Hcy and dose-dependent decrease in DNMT3b expression induced against Hcy, which showed a negative correlation between miR29b and DNMT3b.

In our and other previous reports, it was observed that Hcy activates proteases along with the free radicals that attack membranes.[35–37] Among different proteases, MMPs (MMP2, MMP9) are reported for inducing various molecular cascades in cerebral complications.[23,28,38] Hence, it was interesting to see, whether there is a correlation between MMP9, DNMT3b, and miR29b. We found a dose-dependent increase in MMP9 expression and activity with Hcy. Putting these three together, we postulated that miR29b regulates DNMT3b that can regulate MMP9 expression by methylation. The association of MMP9 gene expression with DNMT3b was indicated by one report in heart that explained that methylation of MMP9 promoter region is correlated with DNMT3b expression.[39] The authors established that with increase in the DNMT3b expression, there is hypermethylation of the MMP9 promoter region, which leads to decrease in the expression of MMP9 genes and *vice versa*. To strongly establish the link between DNMT3b and MMP9, we used DNMT3b siRNA and looked into the expression of MMP9 in bEnd.3 cells. We found that in the presence of DNMT3b siRNA, DNMT3b protein expression was significantly decreased and MMP9 protein expression was significantly increased, as compared to control (Supplementary Figure 1). In order to validate the role of miR29b in regulating DNMT3b and consequently MMP9, we used miR29b mimics and inhibitors. The use of miR29b mimics caused further downregulation of DNMT3b and activation of MMP9 that eventually raised endothelial cell permeability. On the contrary, antagomiR29b led to increase of DNMT3b and decrease in MMP9 enzyme activity, which mitigated cell permeability. These results confirmed that miR29b regulates the levels of DNMT3b, which in turn regulates MMP9

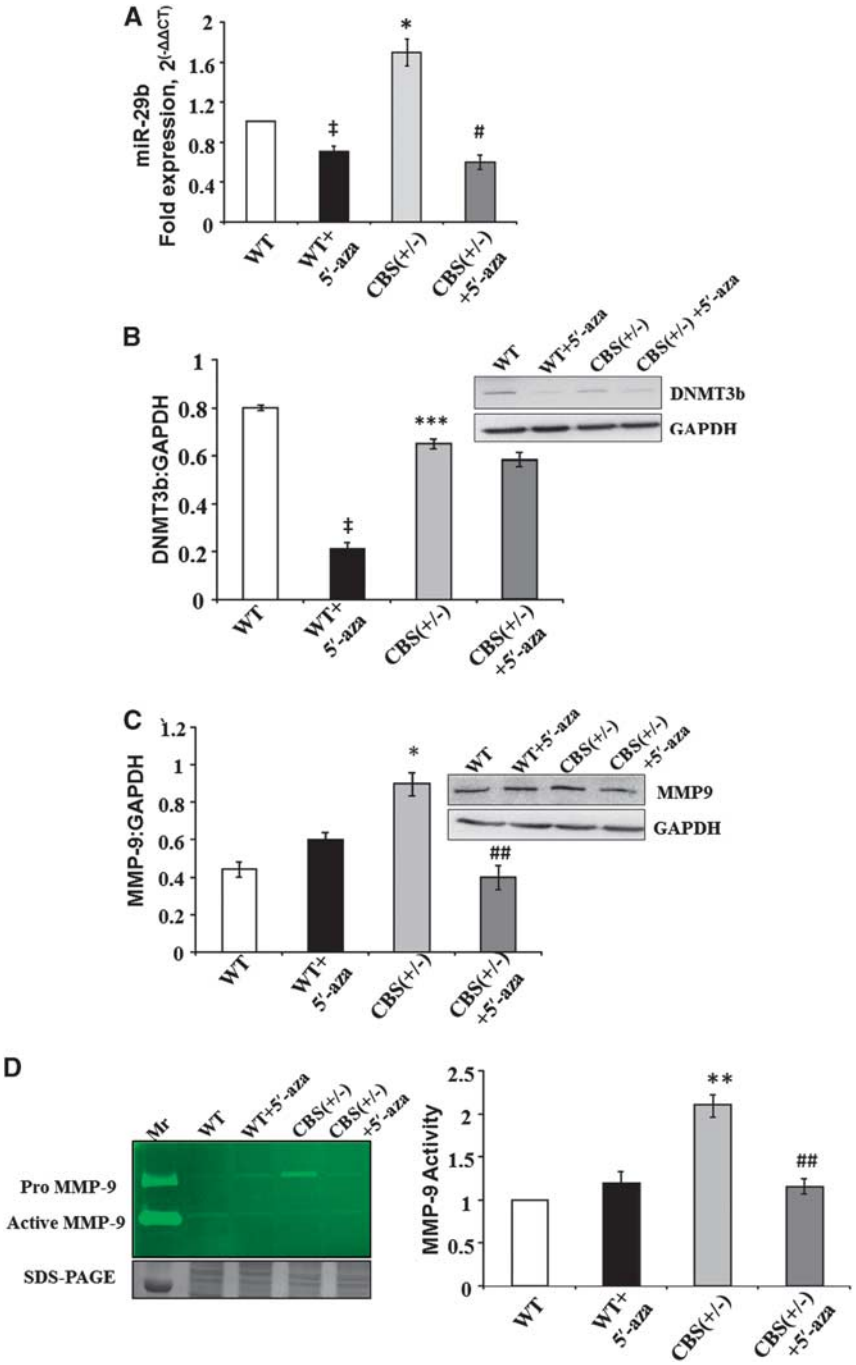

Figure 6. The regulation of miR29, DNMT3b, and MMP9 in mice brain tissues. (**A**) Bar graph showing qPCR analysis for miR29b in wild type (WT), WT + 5′-aza (5′-azacytidine), cystathionine-beta-synthase deficient ($CBS^{+/-}$), and $CBS^{+/-}$ + 5′-aza mice groups. (**B**) Representative western blot image and bar graph showing DNMT3b expression in different mice groups. Glyceraldehyde 3-phosphate dehydrogenase (western blot) and 18sRNA (qPCR) were used as normalization control. (**C**) Representative western blot image and bar graph showing MMP9 expression in different mice groups. Glyceraldehyde 3-phosphate dehydrogenase was used as normalization control. (**D**) Representative gelatin zymography image for MMP9 activity in different mice groups. The loading of the protein sample per lane is confirmed by sodium dodecyl sulfate polyacrylamide gel electrophoresis bands given at the bottom of gelatin zymograph image. The MMP9 activity results are also expressed in bar diagram. Data represent mean ± s.e.m. $^{‡}P<0.05$ versus WT group; $^{*}P<0.05$, $^{**}P<0.005$, $^{***}P<0.0005$ versus WT and WT + 5′-aza groups; $^{\#}P<0.05$, $^{\#\#}P<0.005$ versus $CBS^{+/-}$ groups; data analyzed from four independent experiments ($n=4$).

expression along with its activity and these events regulate cell permeability.

Next, we confirmed our *in vitro* results in the *in vivo* system by correlating the expression of miR29b directly with brain vessel permeability in mice. The intravital fluorescence microscopy analysis revealed increased brain pial venular permeability in $CBS^{+/-}$ mice as compared to WT. We found increased expression of miR29b, and decreased expression of DNMT3b in $CBS^{+/-}$ as compared to WT mice group. In addition, the MMP9 activity and expression were also high in $CBS^{+/-}$ mice in relation to WT littermates. Hence, WT mice, which have less brain vessel permeability, showed decrease in miR29b levels,

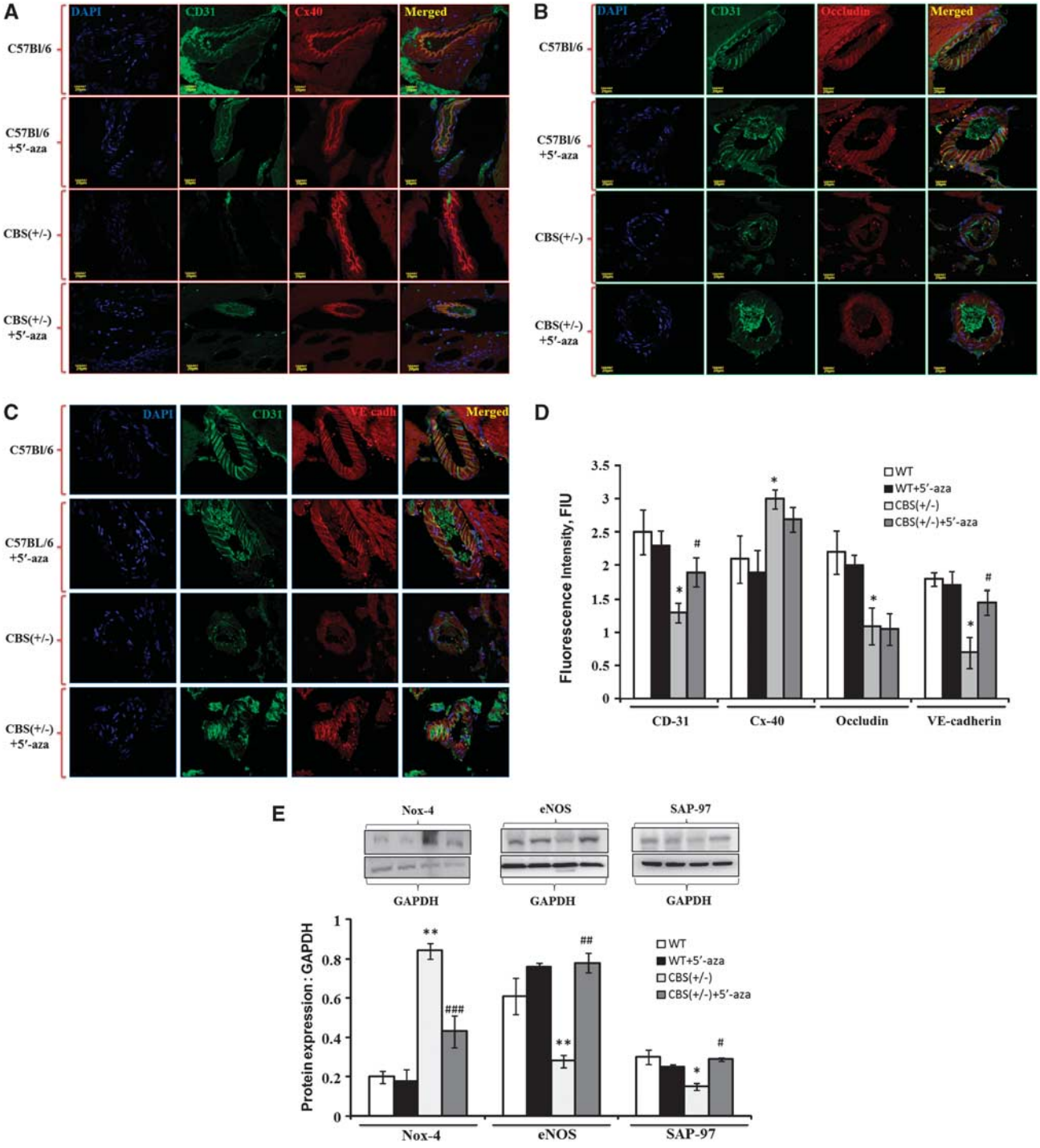

Figure 7. Analysis of molecular and junction protein alterations maintaining blood–brain barrier permeability. (**A**–**C**) Confocal images showing expressions of CD31 (**A**–**C**; green color), connexin40 (**A**, red color), occludin (**B**, red color), and VE-cadherin (**C**, red color) in wild type (WT), WT + 5′-aza (5′-azacytidine), cystathionine-beta-synthase deficient ($CBS^{+/-}$), and $CBS^{+/-}$ + 5′-aza mice brain vessels. Cell nuclei were stained with 4′,6-diamidino-2-phenylindol (DAPI) (blue) and shown in left most panel (**A**–**C**). Merged images are shown in right most panels (**A**–**C**). (**D**) Bar graph shows quantitative estimation of CD31, connexin40, occludin, and VE-cadherin protein intensities in cortical brain vessels and the values are expressed as fluorescence intensity (FIU). (**E**) Bar graph showing NOX-4, eNOS, and SAP-97 protein expressions in different mice groups. Representative western blot images are given at the top of their respective bar diagram. Data represent mean ± s.e.m. $^{*}P<0.05$, $^{**}P<0.05$ versus WT, WT + 5′-aza groups; $^{\#}P<0.05$, $^{\#\#}P<0.005$, $^{\#\#\#}P<0.0005$— versus $CBS^{+/-}$ group; data analyzed from three independent experiments ($n=3$).

which correlated with the expression of DNMT3b and MMP9. To strengthen our hypothesis, we administered locked nucleic acid-anti-miR29b injection *in vivo* to conclusively show miR29b regulation in BBB permeability. We administered scramble miR and anti-miR29b into $CBS^{+/-}$ mice through intracerebral route, as explained by Krutzfeldt *et al.*[40] The author described that local administration of antagomiR-16 is effective as compared with systemic infusions, most likely because of inability of

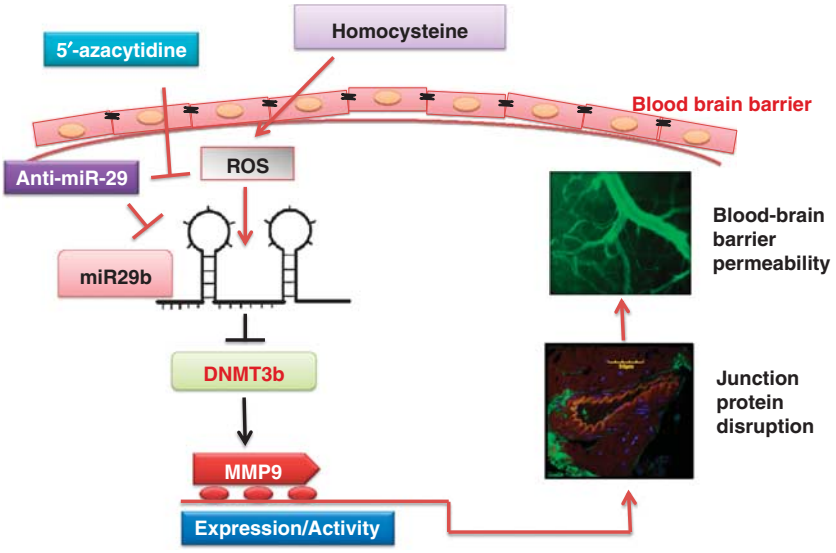

Figure 8. Hypothesis: The figure represents the proposed hypothesis for miR29b-induced mechanism in blood-barrier dysfunction. High levels of homocysteine in blood lead to increase in oxidative stress and miR29b that mediate the opening of blood–brain barrier (BBB) by directly targeting DNMT3b, which then target MMP9. The open BBB thereby influences permeability of the brain vessels and hence leads to BBB dysfunction. 5′-azacytidine improves blood–brain permeability by reducing miR29b and alleviating DNMT3b and MMP9 levels.

oligonucleotides to cross the blood–brain barrier.[40] As compared to $CBS^{+/-}$ + scramble miR mice, $CBS^{+/-}$ + anti-miR29b mice showed significant decrease in miR29b levels along with considerable decrease in FITC-BSA leakage through brain pial venules (Supplementary Figure 2). In agreement to our finding, Zhou *et al.*[41] also found miR29 family member 'miR29a' involvement in the regulation of intestinal membrane permeability in patients with irritable bowel disease.[41] Further, we studied cause–effect relation of miR29b induction with the expression levels of junction proteins that maintain BBB integrity along with oxidative stress and other molecular events *in vivo* (HHcy) mice model. Compared with WT, HHcy mice brain indicated signs of oxidative stress (gain of NOX-4), drop in endothelial function (loss of eNOS), and diminish synaptic plasticity (SAP-97). Apart from that, cortical brain vessels of $CBS^{+/-}$ mice showed distorted expressions of endothelial lining (CD31), gap junctions (Connexin40), tight junction (occludin), and adherent junction (VE-cadherin) as compared to WT mice. All these events confirmed BBB disruption in HHcy mice brain.

As 5′-aza is being used to epigenetically reprogram the endogenous cells and ameliorate neurologic outcome and neuropathic pain,[15,16,42] it was interesting to see the effect of this drug on brain vessel permeability. Interestingly, we found improvement in the BBB permeability in $CBS^{+/-}$ + 5′-aza mice as compared to $CBS^{+/-}$ mice. 5′-aza significantly ameliorated CD31 and VE-cadherin expressions but not the Connexin40 and occludin expressions, which indicated its effect on adherent and endothelial junctions in HHcy mice brain. Hence, the improvement of BBB permeability in $CBS^{+/-}$ + 5′-aza mice brains is probably because of alleviations of endothelial and adherent junctions. In the current report, we used 5′-aza in parallel with Hcy in all the treatment groups (*in vitro* and *in vivo*) to see that whether the effects of 5′-aza involve miR29b. We found that 5′-aza alleviated HHcy-induced oxidative stress and epigenetic changes. In support to our study, Zhang *et al.*[43] have shown that 5′-aza reverts the effects of H_2O_2 induced oxidative stress and epigenetic changes.[43] We also found that in 5′-aza-treated groups, the MMPs activity was decreased (which was upregulated in HHcy), along with amelioration in the expression level of DNMT3b. As the expression of miR29b was also decreased in all 5′-aza-treated groups and hence; we postulate the effects of 5′-aza on BBB permeability are mediated by miR29b. Till date, there are no studies on the role of miR29b in BBB permeability and the effect of 5′-aza on brain vessel permeability. On the basis of results obtained, we have proposed a hypothesis (Figure 8) that explains the regulation of miR29b in HHcy and further downstream events leading to the regulation of MMP9 through DNMT3b.

In summary, our study provides a novel insight into our understanding of the role of microRNAs, especially miR29b in epigenetic modulation of the BBB disruption, as, till date there are no studies on the role of miR29b in BBB permeability and the effect of 5′-aza on brain vessel permeability. The elaboration of Hcy-induced faulty epigenetics explains the pathogenesis of cerebrovascular complications in people who are 'at risk' having high Hcy levels in their blood. Our data explains Hcy-induced BBB permeability epigenetically, and the results reflect that miRNA, DNMTs, and MMPs are involved profoundly in the pathogenesis of leaky cerebral vasculature. The project also paves the way for the future studies on the epigenetic therapy by directing potential microRNA involved in the pathologic process of cerebral diseases.

DISCLOSURE/CONFLICT OF INTEREST

The authors declare no conflict of interest.

REFERENCES

1 Abbott NJ, Ronnback L, Hansson E. Astrocyte-endothelial interactions at the blood-brain barrier. *Nat Rev Neurosci* 2006; **7**: 41–53.
2 Ballabh P, Braun A, Nedergaard M. The blood-brain barrier: an overview: structure, regulation, and clinical implications. *Neurobiol Dis* 2004; **16**: 1–13.
3 Rhodehouse BC, Mayo JN, Beard Jr RS, Chen CH, Bearden SE. Opening of the blood-brain barrier before cerebral pathology in mild hyperhomocysteinemia. *PLoS One* 2013; **8**: e63951.
4 Liu WY, Wang ZB, Zhang LC, Wei X, Li L. Tight junction in blood-brain barrier: an overview of structure, regulation, and regulator substances. *CNS Neurosci Ther* 2012; **18**: 609–615.
5 Fabbri M, Garzon R, Cimmino A, Liu Z, Zanesi N, Callegari E *et al.* MicroRNA-29 family reverts aberrant methylation in lung cancer by targeting DNA methyltransferases 3A and 3B. *Proc Natl Acad Sci USA* 2007; **104**: 15805–15810.

6 Garzon R, Liu S, Fabbri M, Liu Z, Heaphy CE, Callegari E *et al*. MicroRNA-29b induces global DNA hypomethylation and tumor suppressor gene reexpression in acute myeloid leukemia by targeting directly DNMT3A and 3B and indirectly DNMT1. *Blood* 2009; **113**: 6411–6418.
7 Khanna S, Rink C, Ghoorkhanian R, Gnyawali S, Heigel M, Wijesinghe DS *et al*. Loss of miR-29b following acute ischemic stroke contributes to neural cell death and infarct size. *J Cereb Blood Flow Metab* 2013; **33**: 1197–1206.
8 Shi G, Liu Y, Liu T, Yan W, Liu X, Wang Y *et al*. Upregulated miR-29b promotes neuronal cell death by inhibiting Bcl2L2 after ischemic brain injury. *Exp Brain Res* 2012; **216**: 225–230.
9 Beard Jr RS, Bearden SE. Vascular complications of cystathionine beta-synthase deficiency: future directions for homocysteine-to-hydrogen sulfide research. *Am J Physiol Heart Circ Physiol* 2011; **300**: H13–H26.
10 Lominadze D, Roberts AM, Tyagi N, Moshal KS, Tyagi SC. Homocysteine causes cerebrovascular leakage in mice. *Am J Physiol Heart Circ Physiol* 2006; **290**: H1206–H1213.
11 Kamath AF, Chauhan AK, Kisucka J, Dole VS, Loscalzo J, Handy DE *et al*. Elevated levels of homocysteine compromise blood-brain barrier integrity in mice. *Blood* 2006; **107**: 591–593.
12 Qipshidze N, Metreveli N, Lominadze D, Tyagi SC. Folic acid improves acetylcholine-induced vasoconstriction of coronary vessels isolated from hyperhomocysteinemic mice: an implication to coronary vasospasm. *J Cell Physiol* 2011; **226**: 2712–2720.
13 Tyagi SC, Lominadze D, Roberts AM. Homocysteine in microvascular endothelial cell barrier permeability. *Cell Biochem Biophys* 2005; **43**: 37–44.
14 Kalani A, Kamat PK, Tyagi SC, Tyagi N. Synergy of homocysteine, microRNA, and epigenetics: a novel therapeutic approach for stroke. *Mol Neurobiol* 2013; **48**: 157–168.
15 Kang SK, Lee DH, Bae YC, Kim HK, Baik SY, Jung JS. Improvement of neurological deficits by intracerebral transplantation of human adipose tissue-derived stromal cells after cerebral ischemia in rats. *Exp Neurol* 2003; **183**: 355–366.
16 Lee TH, Yoon JG. Intracerebral transplantation of human adipose tissue stromal cells after middle cerebral artery occlusion in rats. *J Clin Neurosci* 2008; **15**: 907–912.
17 Blum W, Garzon R, Klisovic RB, Schwind S, Walker A, Geyer S *et al*. Clinical response and miR-29b predictive significance in older AML patients treated with a 10-day schedule of decitabine. *Proc Natl Acad Sci USA* 2010; **107**: 7473–7478.
18 Yang H, Fang Z, Wei Y, Hu Y, Calin GA, Kantarjian HM *et al*. Levels of miR-29b do not predict for response in patients with acute myelogenous leukemia treated with the combination of 5-azacytidine, valproic acid, and ATRA. *Am J Hematol* 2011; **86**: 237–238.
19 Brown RC, Morris AP, O'Neil RG. Tight junction protein expression and barrier properties of immortalized mouse brain microvessel endothelial cells. *Brain Res* 2007; **1130**: 17–30.
20 Watanabe T, Dohgu S, Takata F, Nishioku T, Nakashima A, Futagami K *et al*. Paracellular barrier and tight junction protein expression in the immortalized brain endothelial cell lines bEND.3, bEND.5 and mouse brain endothelial cell 4. *Biol Pharm Bull* 2013; **36**: 492–495.
21 Muradashvili N, Tyagi R, Lominadze D. A dual-tracer method for differentiating transendothelial transport from paracellular leakage *in vivo* and *in vitro*. *Front Physiol* 2012; **3**: 166.
22 Munjal C, Tyagi N, Lominadze D, Tyagi SC. Matrix metalloproteinase-9 in homocysteine-induced intestinal microvascular endothelial paracellular and transcellular permeability. *J Cell Biochem* 2012; **113**: 1159–1169.
23 Kalani A, Kamat PK, Givvimani S, Brown K, Metreveli N, Tyagi SC *et al*. Nutri-epigenetics ameliorates blood-brain barrier damage and neurodegeneration in hyperhomocysteinemia: role of folic acid. *J Mol Neurosci* 2013; **52**: 202–215.
24 Tyagi N, Moshal KS, Sen U, Vacek TP, Kumar M, Hughes Jr WM *et al*. H2S protects against methionine-induced oxidative stress in brain endothelial cells. *Antioxid Redox Signal* 2009; **11**: 25–33.
25 Tyagi N, Qipshidze N, Sen U, Rodriguez W, Ovechkin A, Tyagi SC. Cystathionine beta synthase gene dose dependent vascular remodeling in murine model of hyperhomocysteinemia. *Int J Physiol Pathophysiol Pharmacol* 2011; **3**: 210–222.
26 Krutzfeldt J, Rajewsky N, Braich R, Rajeev KG, Tuschl T, Manoharan M *et al*. Silencing of microRNAs *in vivo* with 'antagomirs'. *Nature* 2005; **438**: 685–689.
27 Elmen J, Lindow M, Schutz S, Lawrence M, Petri A, Obad S *et al*. LNA-mediated microRNA silencing in non-human primates. *Nature* 2008; **452**: 896–899.
28 Kamat PK, Kalani A, Givvimani S, Sathnur PB, Tyagi SC, Tyagi N. Hydrogen sulfide attenuates neurodegeneration and neurovascular dysfunction induced by intracerebral-administered homocysteine in mice. *Neuroscience* 2013; **252**: 302–319.
29 Moustapha A, Gupta A, Robinson K, Arheart K, Jacobsen DW, Schreiber MJ *et al*. Prevalence and determinants of hyperhomocysteinemia in hemodialysis and peritoneal dialysis. *Kidney Int* 1999; **55**: 1470–1475.
30 Ueland PM, Refsum H. Plasma homocysteine, a risk factor for vascular disease: plasma levels in health, disease, and drug therapy. *J Lab Clin Med* 1989; **114**: 473–501.
31 Hassan A, Hunt BJ, O'Sullivan M, Bell R, D'Souza R, Jeffery S *et al*. Homocysteine is a risk factor for cerebral small vessel disease, acting via endothelial dysfunction. *Brain* 2004; **127**: 212–219.
32 Kumar M, Tyagi N, Moshal KS, Sen U, Pushpakumar SB, Vacek T *et al*. GABAA receptor agonist mitigates homocysteine-induced cerebrovascular remodeling in knockout mice. *Brain Res* 2008; **1221**: 147–153.
33 Beard Jr RS, Reynolds JJ, Bearden SE. Hyperhomocysteinemia increases permeability of the blood-brain barrier by NMDA receptor-dependent regulation of adherens and tight junctions. *Blood* 2011; **118**: 2007–2014.
34 Takada S, Berezikov E, Choi YL, Yamashita Y, Mano H. Potential role of miR-29b in modulation of Dnmt3a and Dnmt3b expression in primordial germ cells of female mouse embryos. *RNA* 2009; **15**: 1507–1514.
35 Rosell A, Alvarez-Sabin J, Arenillas JF, Rovira A, Delgado P, Fernández-Cadenas I *et al*. A matrix metalloproteinase protein array reveals a strong relation between MMP-9 and MMP-13 with diffusion-weighted image lesion increase in human stroke. *Stroke* 2005; **36**: 1415–1420.
36 Tyagi N, Gillespie W, Vacek JC, Sen U, Tyagi SC, Lominadze D. Activation of GABA-A receptor ameliorates homocysteine-induced MMP-9 activation by ERK pathway. *J Cell Physiol* 2009; **220**: 257–266.
37 Moshal KS, Tipparaju SM, Vacek TP, Kumar M, Singh M, Frank IE *et al*. Mitochondrial matrix metalloproteinase activation decreases myocyte contractility in hyperhomocysteinemia. *Am J Physiol Heart Circ Physiol* 2008; **295**: H890–H897.
38 Sudduth TL, Powell DK, Smith CD, Greenstein A, Wilcock DM. Induction of hyperhomocysteinemia models vascular dementia by induction of cerebral microhemorrhages and neuroinflammation. *J Cereb Blood Flow Metab* 2013; **33**: 708–715.
39 Chen KC, Wang YS, Hu CY, Chang WC, Liao YC, Dai CY *et al*. OxLDL up-regulates microRNA-29b, leading to epigenetic modifications of MMP-2/MMP-9 genes: a novel mechanism for cardiovascular diseases. *FASEB J* 2011; **25**: 1718–1728.
40 Krutzfeldt J, Kuwajima S, Braich R, Rajeev KG, Pena J, Tuschl T *et al*. Specificity, duplex degradation and subcellular localization of antagomirs. *Nucleic Acids Res* 2007; **35**: 2885–2892.
41 Zhou Q, Souba WW, Croce CM, Verne GN. MicroRNA-29a regulates intestinal membrane permeability in patients with irritable bowel syndrome. *Gut* 2010; **59**: 775–784.
42 Wang Y, Liu C, Guo QL, Yan JQ, Zhu XY, Huang CS *et al*. Intrathecal 5-azacytidine inhibits global DNA methylation and methyl- CpG-binding protein 2 expression and alleviates neuropathic pain in rats following chronic constriction injury. *Brain Res* 2011; **1418**: 64–69.
43 Zhang R, Kang KA, Kim KC, Na SY, Chang WY, Kim GY *et al*. Oxidative stress causes epigenetic alteration of CDX1 expression in colorectal cancer cells. *Gene* 2013; **524**: 214–219.

Supplementary Information accompanies the paper on the Journal of Cerebral Blood Flow & Metabolism website (http://www.nature.com/jcbfm)